Atmospheric Environment 285 (2022) 119243

Contents lists available at ScienceDirect

Atmospheric Environment

journal homepage: www.elsevier.com/locate/atmosenv

Chemical composition of NR-PM_1 in a coastal city of Southeast China: Temporal variations and formation pathways

Yuping Chen [a,b,c], Chen Yang [a,b,c], Lingling Xu [a,b,*], Jinsheng Chen [a,b,**], Yanru Zhang [d], Jiayan Shi [b], Xiaolong Fan [a,b], Ronghua Zheng [a,b], Youwei Hong [a,b], Mengren Li [a,b]

[a] Center for Excellence in Regional Atmospheric Environment, Institute of Urban Environment, Chinese Academy of Sciences, Xiamen, 361021, China
[b] Key Lab of Urban Environment and Health, Institute of Urban Environment, Chinese Academy of Sciences, Xiamen, 361021, China
[c] University of Chinese Academy of Sciences, Beijing, 100049, China
[d] Xiamen Environmental Monitoring Station, Xiamen, 361021, China

HIGHLIGHTS

- Chemical components in NR-PM_1 in Southeast China during 2017–2020 were presented.
- Formation of sulfate and OOA in summer was dominated by photochemical reactions.
- The dominant pathway for secondary aerosols in winter varied across years.
- Enhanced atmospheric oxidation capacity contributed to the increasing oxidation degree of OA.

ARTICLE INFO

Keywords:
Secondary aerosol
Atmospheric oxidation capacity
Photochemical reaction
Aqueous-phase reaction

ABSTRACT

This study presents the variation of chemical components in non-refractory submicron aerosols (NR-PM_1) measured by Q-ACSM in a coastal city of Southeast China in summer and winter during the years 2017, 2018, and 2020. As we know, long-term data on aerosol chemical composition were scarce in this region. The mass concentration of NR-PM_1 decreased evidently, but the chemical composition of NR-PM_1 showed a minor variation with OA increased and NO_3 decreased over the years. PMF/ME-2 models were performed to identify OA factors resolving POA, less oxidized OOA (LO-OOA), and more oxidized OOA (MO-OOA) in this study. Secondary components made dominant contributions of 85.1%–90.7% to NR-PM_1, and OOA became more important in aerosols with time. The SOR, NOR, and MO-OOA/LO-OOA ratio as a function of LWC and O_x, combined with the diurnal variation of secondary aerosols (SAs), were performed to explore the main formation mechanism of NO_3, SO_4, and OOA. The results indicate that SO_4 and OOA factors in summer were mainly affected by photochemical reactions, while the characteristics and the main formation pathways of NO_3 and OOA factors in winter varied largely across the different years. The oxidized degree of OA had elevated in 2020 compared to 2017 and 2018 as the f_{44} (ratio of m/z 44 to total signal) of OA increased. Our study on the annual variation of aerosol chemical composition and the dominant formation pathways of secondary components will provide a scientific reference for air quality improvement.

1. Introduction

Aerosols are critical to climate change and human health (Heal et al., 2012; IPCC, 2021; Kreyling et al., 2006; Pöschl, 2005). Aerosols mass concentrations in the atmosphere are mainly determined by primary emissions, secondary processes, and meteorological conditions (Bressi et al., 2016; Gu et al., 2020; Sun et al., 2015, 2016; Zhu et al., 2021). Secondary aerosols (SAs) make outstanding contributions to aerosols, e.

* Corresponding author. Center for Excellence in Regional Atmospheric Environment, Institute of Urban Environment, Chinese Academy of Sciences, Xiamen, 361021, China.
** Corresponding author. Center for Excellence in Regional Atmospheric Environment, Institute of Urban Environment, Chinese Academy of Sciences, Xiamen, 361021, China.
E-mail addresses: linglingxu@iue.ac.cn (L. Xu), jschen@iue.ac.cn (J. Chen).

https://doi.org/10.1016/j.atmosenv.2022.119243
Received 20 February 2022; Received in revised form 18 June 2022; Accepted 19 June 2022
Available online 25 June 2022

g. SAs contributed 64%–92% to non-refractory submicron aerosols (NR-PM_1) in major cities of Asia (Zhou et al., 2020). The properties and environmental effects of SAs are distinguishable from those of primary emission aerosols (Li et al., 2017a). For example, the enhanced hygroscopicity of SAs would alter the aerosols scattering and cloud formation ability (Gunthe et al., 2011), thereby affecting visibility and climate. Previous studies have indicated that the aerosols pollution events in China in recent years were caused by the increase of SAs derived mainly from photochemical reactions and aqueous-phase reactions (Huang et al., 2020; Zheng et al., 2015). Severe aerosols pollution events have been reported to be related to high relative humidity (RH) (Hu et al., 2016; Li et al., 2017b). Simultaneously, atmospheric oxidation capacity, usually represents by the concentration of O_x ($NO_2 + O_3$), was reported to be enhanced in recent years and to contribute significantly to the formation of SAs (Lei et al., 2021; Li et al., 2021a; Liu et al., 2021). Therefore, understanding the characteristics and formation pathways of SAs is essential to reduce the mass concentration of aerosols and mitigate its impact on the environment and humans.

The concentrations of SO_2 and NO_2 have reduced substantially due to control policies in recent years, but the contributions of sulfate and nitrate to aerosols were not expected to follow (Huang et al., 2014; Xu et al., 2015). One of the reasons is that the increase in atmospheric oxidation capacity compensated for the reduction of the precursors (Sun et al., 2020). Nitrate was reported as an important driver for aerosols growth, because it had a prominent proportion of aerosols during severe aerosols pollution events (Xiao et al., 2021; Xu et al., 2019; Yang et al., 2021; Zhao et al., 2020). The diurnal trend of sulfate with a peak concentration at midday or afternoon was widely observed, which indicated that photochemical reactions were the dominant pathway of sulfate formation (Dai et al., 2019; Sun et al., 2012; Xu et al., 2014; Zhao et al., 2020). In addition, previous studies have found a rapid increase of sulfate associated with high RH in some aerosols pollution events, suggesting the contribution of aqueous-phase oxidation of SO_2 to sulfate (Hu et al., 2016; Sun et al., 2014; Wang et al., 2014). Nevertheless, the mechanism for SO_2 conversion to sulfate in aerosols is now under discussion, and the opinions are quite controversial (Cheng et al., 2016; Harris et al., 2013; Liu et al., 2020a, 2020b; Wang et al., 2020; Zheng et al., 2020). Due to the complex interactions between gaseous precursors and atmospheric oxidation capacity, the future air quality improvement will also be challenging (Lei et al., 2021; Sun et al., 2020).

Organic aerosol (OA) is the dominant component of NR-PM_1 (Brito et al., 2014; Dai et al., 2019; Zhou et al., 2020). Regarding its origin, OA could be classified into primary OA (POA) and secondary OA (SOA). SOA is resulted from chemical conversion of pre-existing particles, nucleation, or gas-to-particle condensation (Hallquist et al., 2009; Kroll and Seinfeld, 2008). Previous studies have reported that atmospheric photochemical aging reaction is a crucial pathway for the formation and evolution of SOA (An et al., 2019; Chen et al., 2021). Nevertheless, aqueous-phase reactions were found to have a significant influence on the formation of SOA during periods of low atmospheric oxidative capacity (Wang et al., 2017). The results indicate that the formation of SOA via aqueous-phase reactions or photochemical reactions strongly depends on the differences in meteorology and atmospheric oxidation capacity (Dai et al., 2019; Hu et al., 2016; Xu et al., 2017). The oxidation degree of SOA showed a spatial and seasonal variability. Jimenez et al. (2009) found a common trend of the fraction of more oxidized SOA in OA increasing from urban to rural areas. The oxidation degree of SOA was reported to be related to solar radiation and temperature as the ratio of less/more oxidized SOA was low in warm seasons (Via et al., 2021). Besides, it's generally considered that more oxidized SOA had a high contribution to OA in long-distance transport air masses (Gu et al., 2020; Sun et al., 2018). Up to now, the driven formation pathways of oxidized OA remain poorly understood (Xu et al., 2017). Therefore, in-depth analysis of inter-annual and seasonal differences in the formation mechanism of SAs under the impact of distinct emission sources and meteorological conditions would help comprehensively understand the properties of aerosols and improve the accuracy of model simulations.

In this study, an Aerodyne Aerosol Chemical Speciation Monitor (ACSM) with high time resolution was deployed to monitor the chemical composition of NR-PM_1 in Xiamen, a coastal city of Southeast China, in the summer and winter of 2017, 2018, and 2020. Xiamen is the transportation channel of the two most economically developed regions, the Yangtze River Delta and the Pearl River Delta, which is also affected by mixing air masses from continents and marine. As we know, the monitoring data of chemical composition of aerosols in many years were scarce in Southeast China. The PMF/ME-2 method was performed to determine the primary and oxidized OA factors, including primary OA (POA), less-oxidized oxygenated OA (LO-OOA), and more-oxidized oxygenated OA (MO-OOA). The objectives of this study were to (1) describe the seasonal and annual variations of chemical composition of NR-PM_1 in the years of 2017, 2018, and 2020 in Xiamen, Southeast China, (2) identify the main formation pathways of sulfate and nitrate in summer and winter of the different years, and (3) investigate the characteristics of OA factors, the oxidation degree of OA, and the main formation pathways of OOA in the study region.

2. Experimental methods

2.1. Observation site and periods

The field observation site (118°03′E, 24°36′N, 80 m a.s.l) was located in the Institute of Urban Environment, Chinese Academy of Sciences (IUE) in Jimei District, Xiamen (Fig. S1). IUE is a suburban site with two roads 100 m away to the northwest and northeast, respectively. Xiamen is a subtropical city with a warm climate and high RH throughout the year. The prevailing wind is the ocean monsoon from the southeast direction in summer and the land wind from the north and northeast of China in winter. Six field observation campaigns were conducted in August and December, representing summer and winter, respectively. The specific time periods were 1–15 August 2017, 3–31 December 2017, 1–22 August 2018, 1–22 December 2018, 6–31 August 2020, and 1–17 December 2020.

2.2. Observation instruments

Chemical composition of NR-PM_1 including organics aerosol (OA), nitrate (NO_3), sulfate (SO_4), ammonium (NH_4), and chloride (Chl) was measured by an ACSM. The detail of ACSM instrument operation can be found in previous studies (Ng et al., 2011; Sun et al., 2012; Tiitta et al., 2014). Briefly, aerosols were sampled at the main inlet at a flow rate of 3 L min^{-1} and dried using a Nafion dryer system (Perma Pure, New Jersey, USA) to keep the RH below 40% (Sun et al., 2012; Zhao et al., 2020). A subsample flow of 0.085 L min^{-1} passed through a critical orifice and entered an aerodynamic lens that focused the particles into a narrow beam. Particles were then flash-vaporized at 600 °C in high vacuum conditions and ionized by hard-electron impact (70 eV), and the resulting fragments were analyzed by a quadrupole mass spectrometer (Ng et al., 2011). The time resolution of ACSM was about 15 min with a scan from m/z 10–150 amu (atomic mass unit) at 200 m s amu^{-1} rate. The ionization efficiency (IE) and relative ion efficiency (RIE) calibrations were performed using size-selected ammonium nitrate (NH_4NO_3) and ammonium sulfate ($(NH_4)_2SO_4$) particles (300 nm) by a differential mobility analyzer (DMA, TSI Co., US) and counted by a condensation particle counter (CPC) (Ng et al., 2011). The data is corrected using the calibration parameters obtained closest to the observation period. Specifically, the IE was 5.67×10^{-11} for the periods 2017 and 2018 and 4.27×10^{-11} for 2020. The RIE for ammonium and sulfate was 5.69 and 0.8 for the periods 2017 and 2018, 5.49 and 0.53 for 2020. The default RIE values were used for nitrate (1.1), OA (1.4), and chloride (1.3) (Canagaratna et al., 2007; Ng et al., 2011). NH_4NO_3 might induce an overestimation of OA at m/z 44 (Pieber et al., 2016), but the data of this study did not do corrections for m/z 44 for some reasons. Firstly, the

discrepancies in f_{44} result in significant differences in the PMF factor profile analysis but not in the total factor contribution (Fröhlich et al., 2015). Secondly, previous studies on Q-ACSM measurement have reported the interference of ammonium nitrate to f_{44} was 7.54 ± 0.63% (Pieber et al., 2016) and 3.6%–7.8% (Tobler et al., 2021) relative to nitrate. Considering that NH_4NO_3 fractions are typically low compared to OA for ambient data sets, the influence of ammonium nitrate on f_{44} might be minor.

Hourly $PM_{2.5}$ concentration was determined using a continuous particulate monitor (TEOM 1405-D, Thermo Co., USA) by the method of tapered element oscillating microbalance. Carbon oxide (CO), ozone (O_3), sulfur dioxide (SO_2), and nitrogen oxides (NO_x) were measured by gas analyzers (Thermo Fisher Scientific, Waltham, MA, USA). Black carbon (BC) was determined with model AE-31 Aethalometer (Magee Co., USA). The concentration of BC used in this study was detected at 880 nm with a time resolution of 5 min. Temperature (*T*), RH, solar radiation (SR), and ultraviolet (UV) were obtained from an automatic air station of Xiamen. The detailed meteorological data for each summer and winter in the three different years could be referred to Table 1.

2.3. ACSM data analysis

The data of ACSM was analyzed with the standard Wave Metrics Igor Pro based data analysis software (version 6.37). The data analysis protocols were referred to the previous studies (Sun et al., 2012; Wang et al., 2017). The collection efficiency (CE) values were calculated using algorithms described by Middlebrook et al. (2012). The yielded composition-dependent CEs ranged from 0.46 ± 0.02 to 0.51 ± 0.08.

Positive matrix factorization (PMF) was applied to identify the OA factors with the Igor Pro based PMF evaluation toolkit (PET) by analyzing the high time resolution mass spectra (Paatero and Tapper, 1994; Ulbrich et al., 2009). The OA factors of 2020 derived from the PMF all showed unexpected high f_{44} values compared to the results of 2017 and 2018. Thus, we further constrained the POA of 2020 by SoFi (version 6.G) along with the multi-linear engine (ME-2) algorithm (Canonaco et al., 2013). Specifically, we used the average spectra profile of POA in 2017–2018 as constraints to analyze the source of organic matrices in 2020. The constraint value (a-value) was selected from 0 to 1 with 0.1 as an interval.

In this study, PMF/ME-2 analysis of OA mass spectra resolved three OA factors including POA, LO-OOA, and MO-OOA (Fig. S2). The identification of OA factors was verified by distinguishing mass spectrum, analyzing diurnal variation of the factors, and comparing the time series of the factors and external tracers (Paatero and Tapper, 1994). In this study, only values of $m/z < 120$ were used, because the fraction of signals $m/z > 120$ in total signals was minor and the uncertainties of $m/z > 120$ were large (Sun et al., 2012; Zhang et al., 2020). The large uncertainty above m/z 120 was likely caused by the low ion transmission efficiency and the large interferences of naphthalene signals on some m/z's (e.g., m/z 127, 128, and 129). "Bad" ions with a signal-to-noise ratio (SNR) < 0.2 were removed, while "weak" ions with a SNR of 0.2–2 were down-weighted by a factor of 2.

2.4. Estimation of aerosol liquid water contents (LWC)

Liquid water contents (LWC) can be contributed from both inorganic species (W_i) and organic species (W_o). The thermodynamic model ISORROPIA-II has been extensively used to predict W_i (Fountoukis and Nenes, 2007). In this study, the input of ISORROPIA included meteorological data (RH, *T*), the mass concentration of inorganic components (NO_3, SO_4, NH_4, and Chl) from ACSM, and Na^+, K^+, Ca^{2+}, Mg^{2+}, and gas-phase NH_3 was measured by MARGA ADI 2080 (Metrohm, Switzerland). Forward mode and metastable were adopted in this study. W_o were calculated based on an aerosol hygroscopicity parameter, describing as follows (Petters and Kreidenweis, 2007):

$$W_o = \frac{m_{OA}\rho_w}{\rho_{OA}} \times \frac{k_{OA}}{\left(\frac{1}{RH} - 1\right)} \quad (1)$$

where m_{OA} is the organic aerosol mass concentration from ACSM. ρ_w is water density, and a typical organic density (ρ_{OA}) of 1.4 g cm^{-3} is used (Kuwata et al., 2011), k_{OA} is calculated by the result of 2.10 × f_{44} - 0.11 (Mei et al., 2013), which results in the average values of 0.15 ± 0.04 for summer and winter 2017, 0.16 ± 0.05 for summer 2018, 0.20 ± 0.05 for winter 2018, 0.29 ± 0.09 for summer 2020, and 0.31 ± 0.08 for winter 2020 in this study. As shown in Fig. S4, LWC present a positive trend as a function of RH in all six periods.

Table 1
Concentrations (mean ± sd) of NR-PM_1, chemical components, gaseous pollutants, and meteorological parameters in six observation periods.

	Summer 2017	winter 2017	Summer 2018	Winter 2018	Summer 2020	Winter 2020
NR-PM_1	21.0 ± 7.6	24.5 ± 12.7	18.6 ± 9.6	19.5 ± 15.9	10.1 ± 5.7	13.6 ± 9.8
$PM_{2.5}$	32.9 ± 9.5	42.7 ± 19.6	20.1 ± 9.5	35.0 ± 24.3	18.0 ± 8.8	21.6 ± 18.2
Components (μg m^{-3})						
OA	9.64 ± 3.94	9.94 ± 4.97	7.89 ± 4.90	8.42 ± 6.04	5.24 ± 3.04	6.28 ± 4.28
NO_3	2.16 ± 1.79	6.13 ± 4.72	2.51 ± 2.23	4.63 ± 5.43	0.74 ± 0.80	2.73 ± 3.53
SO_4	6.56 ± 2.02	4.92 ± 1.95	5.55 ± 2.96	3.55 ± 2.35	3.03 ± 1.88	2.71 ± 1.40
NH_4	2.46 ± 0.87	3.02 ± 1.63	2.49 ± 1.27	2.50 ± 2.29	1.02 ± 0.66	1.35 ± 1.05
Chl	0.21 ± 0.19	0.45 ± 0.44	0.13 ± 0.13	0.36 ± 0.43	0.05 ± 0.05	0.17 ± 0.19
BC	2.10 ± 0.84	1.42 ± 0.69	1.47 ± 0.76	1.86 ± 1.21	0.88 ± 0.53	0.65 ± 0.38
Gaseous pollutants (μg m^{-3})						
CO (mg m^{-3})	0.44 ± 0.17	0.49 ± 0.16	0.58 ± 0.14	0.60 ± 0.15	0.48 ± 0.11	0.54 ± 0.17
SO_2	6.1 ± 4.8	9.4 ± 5.9	6.1 ± 3.1	13.2 ± 4.0	4.7 ± 3.0	15.6 ± 2.2
NO_2	26.9 ± 14.8	35.5 ± 19.0	30.5 ± 15.4	44.1 ± 22.3	18.4 ± 12.1	10.0 ± 6.8
NO_x	35.1 ± 24.1	44.9 ± 36.3	43.7 ± 38.1	59.5 ± 44.6	29.3 ± 21.2	15.1 ± 10.8
O_3	58.9 ± 49.2	59.9 ± 34.0	61.5 ± 55.2	39.0 ± 29.9	46.3 ± 40.9	45.7 ± 23.8
O_x	86.0 ± 40.0	95.3 ± 28.6	91.0 ± 47.6	82.9 ± 31.5	64.6 ± 38.5	53.9 ± 21.8
Meteorology						
T (°C)	30.3 ± 2.4	16.3 ± 2.7	29.7 ± 2.1	18.7 ± 3.2	30.1 ± 2.6	17.6 ± 2.9
RH (%)	82.9 ± 9.5	64.9 ± 13.2	80.6 ± 9.7	78.0 ± 11.7	71.9 ± 11.1	67.6 ± 9.6
SR (w m^{-2})	215 ± 284	126 ± 192	228 ± 304	–	–	–
UV (w m^{-2})	–	6.4 ± 10.0	12.7 ± 16.9	6.5 ± 10.1	12.8 ± 16.8	5.3 ± 8.9
Other parameters						
SOR	0.46 ± 0.17	0.30 ± 0.12	0.38 ± 0.12	0.14 ± 0.07	0.32 ± 0.20	0.10 ± 0.05
NOR	0.06 ± 0.04	0.12 ± 0.07	0.06 ± 0.04	0.06 ± 0.05	0.04 ± 0.03	0.18 ± 0.15

Note: NO_x is the sum of NO and NO_2. O_x is the sum of O_3 and NO_2. *T*: temperature, RH: relative humidity, SR: solar radiation. UV: ultraviolet. SOR: sulfur oxidation rate. NOR: nitrogen oxidation rate.

3. Results and discussion

3.1. Temporal variations of NR-PM_1

The average mass concentrations of NR-PM_1 at the observation site were 21.0, 18.6, and 10.1 μg m^{-3} in summer and 24.5, 19.5, and 13.6 μg m^{-3} in winter in the years of 2017, 2018, and 2020. The total PM_1 (NR-PM_1 + BC) and $PM_{2.5}$ concentrations were closely correlated (r = 0.89–0.95). The slopes of PM_1 vs. $PM_{2.5}$ were 0.79, 0.99, and 0.65 in summer relative to 0.71, 0.65, and 0.50 in winter of 2017, 2018, and 2020, respectively. The NR-PM_1 concentrations in winter were significantly higher than those in summer ($p < 0.001$, *T*-test). Moreover, the NR-PM_1 concentrations changed more drastically in winter (coefficient of variation, CV = 0.52, 0.81, and 0.72) than in summer (CV = 0.36, 0.52, and 0.57). As shown in Fig. 1a, the concentration of NR-PM_1 showed a decreasing trend from 2017 to 2020. The decreases in summer were 11.4% from 2017 to 2018 and 45.7% from 2018 to 2020, while in winter, they were 20.4% and 30.1% respectively. The average wind speeds in summer and winter for the three years are comparable, with an average value of <2.0 m s^{-1}. The boundary layer height (BLH) was comparable in three summers, while the BLH was extremely high in winter 2020 (719 m) relative to winter 2017 (577 m) and 2018 (415 m), which could partly contribute to low PM_1 concentration in winter 2020.

The average concentration of individual chemical components in NR-PM_1 generally showed a decreasing trend among years. The concentrations of OA, NH_4, and Chl showed a minor seasonal variation. Whereas the concentrations of NO_3 and SO_4 were significantly different between summer and winter ($p < 0.001$, *T*-test). Specifically, NO_3 concentrations in winter of 2017, 2018, and 2020 were 2.8, 1.8, and 3.7 times than those in summer, while SO_4 concentrations were obviously elevated in summer compared to winter.

OA was the dominant chemical component in NR-PM_1, with a proportion of 40.6%–52.0% over the six observation periods. The OA proportions in NR-PM_1 of this study are similar to the results reported from Guangzhou (45%–53%), Beijing (40%–51%), and Shanghai (43%–51%) (Guo et al., 2020; Sun et al., 2015; Zhu et al., 2021). As shown in Fig. 1b, the proportion of OA significantly increased and the proportion of NO_3 decreased in 2020 relative to the previous two years, whereas the proportion of SO_4 was stable from year to year. There was a minor difference (<5%) in the proportion of OA in NR-PM_1 between summer and winter. Secondary inorganic aerosols (SIA, include SO_4, NO_3, and NH_4) had an outstanding contribution to NR-PM_1. The SIA was dominated by sulfate (taking 29.9%–30.2% of NR-PM_1) in summer, while the proportion of nitrate elevated in winter (20.6%–25.1%) and became the dominant SIA species. In addition, the proportion of NH_4 (10.0%–13.4%) in NR-PM_1 did not show a pronounced difference among the years and seasons in this study. The proportion of Chl in NR-PM_1 was relatively small (0.5%–1.9%). It is important to note that the measurement of Chl was subject to large uncertainties due to very low concentrations and potential determination problems (Tobler et al., 2020).

3.2. Formation pathways of sulfate and nitrate

The contribution of SO_4 and NO_3 to NR-PM_1 had a minor difference among years but a significant difference between seasons. The mass concentration of SO_4 and its proportion in NR-PM_1 were remarkably higher in summer than in winter, while the seasonal variations of NO_3 were exactly opposite. The seasonality of SO_4 and NO_3 in the study region is consistent with the results of previous studies conducted in Houston, USA (Dai et al., 2019), Marseille, France (Chazeau et al., 2021), Xinglong, the North China Plain (Li et al., 2021b), and Shanghai, the Yangtze River Delta of China (Zhao et al., 2020; Zhu et al., 2021), but different from those in Beijing (Gu et al., 2020; Hu et al., 2016).

3.2.1. Sulfate

In this study, the higher SO_4 concentration in winter than in summer (Table 1) was inconsistent with the seasonality of SO_2. Sulfur oxidation rate ($SOR = [SO_4]/([SO_4] + [SO_2])$, [x] is molar concentration) was calculated to determine the degree of the oxidation of SO_2 to SO_4. The SOR values in the summer of 2017, 2018, and 2020 (0.46, 0.38, and 0.32) were all remarkably higher than those in winter (0.30, 0.14, and 0.10, Table 1). The seasonality of SO_2 and SOR suggests that the elevated SO_4 concentration and its proportion in NR-PM_1 in summer might be mainly contributed by the formation process of SO_4. As shown in Fig. 2, the SOR in the summer of 2018 and 2020 increased with the increase of O_x within the observed range. In this study, the sulfate concentration in the summer of 2018 and 2020 peaked around midday, just after its precursor SO_2 (Figs. S5 and 6). The daytime peak of sulfate in summer has been reported in a number of previous studies (Xu et al., 2014; Yang et al., 2020; Zhou et al., 2010). This phenomenon could be ascribed to the photochemical formation of sulfate, although it was also contributed by the advection of sulfate from cloud chemistry. The relationship between SOR and O_x and the diurnal pattern of sulfate suggest a promotion effect of photochemical reactions on the conversion of SO_2 to SO_4, which was likely responsible for the elevated SO_4 concentration in the summer of 2018 and 2020 despite the precursor SO_2 was low.

Differently, the SOR in summer 2017 did not show a distinct trend with O_x (Fig. 2) and the highest SOR values presented in the case of extremely high RH (>85%). In addition, the sulfate concentrations in summer 2017 increased over night and peaked in the early morning (Fig. S5). The summer of 2017 was characterized by higher RH than the summer of 2018 and 2020, and the diurnal highest RH (~90%, Fig. S7) occurred in the early morning. Thus, we could speculate that an important contribution of aqueous-phase reactions to the formation of

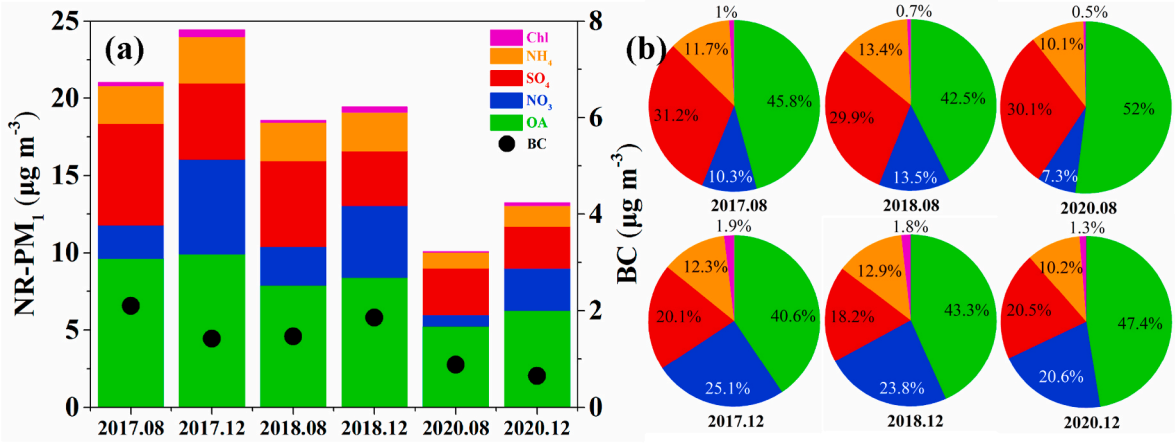

Fig. 1. Monthly average of chemical composition (a) and its proportion (b) in NR-PM_1.

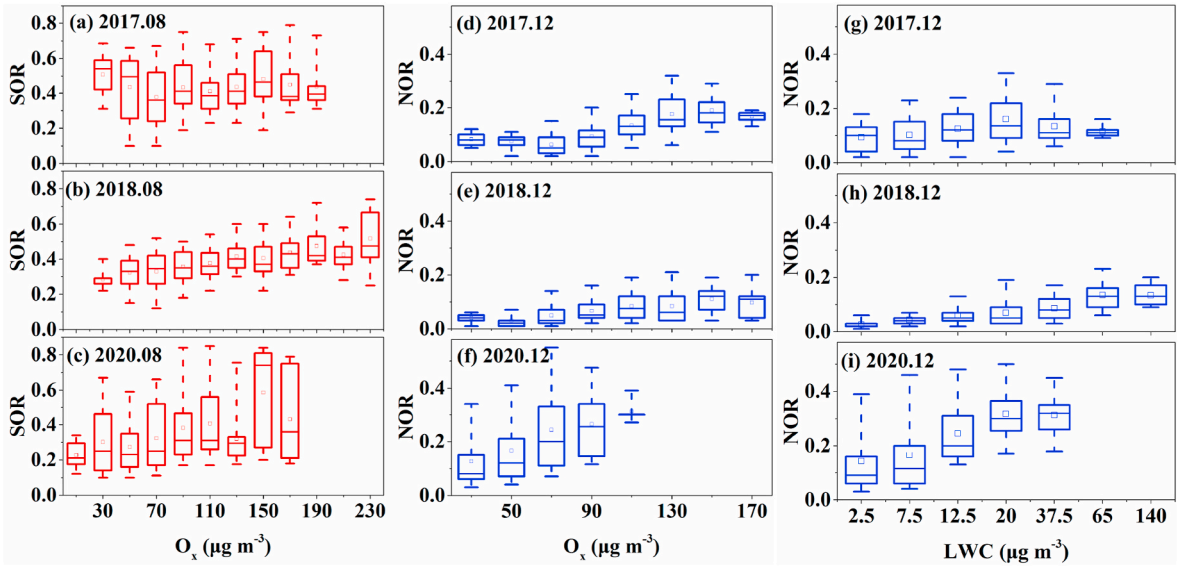

Fig. 2. Summer SOR and winter NOR as a function of O_x and LWC in 2017, 2018, and 2020. Mean (square), median (horizontal line), 25th and 75th percentiles (lower and upper box lines), and 5th and 95th percentiles (lower and upper whiskers) are displayed in the box.

sulfate and eventually to the elevated SO_4 in summer 2017.

3.2.2. Nitrate

Nitrogen oxidation rate ($NOR = [NO_3]/([NO_3] + [NO_2])$) was also calculated to determine the degree of the oxidation of NO_2 to NO_3. The seasonal variation of NO_3 with higher concentrations in winter than in summer was partly contributed by the seasonal fluctuations of BLH. What's more, the high temperature in summer would lead to a rapid decomposition of nitrate, which suppresses the partitioning of nitrate from gas to the particulate phase (Meng et al., 2011; Seinfeld and Pandis, 2016; Sun et al., 2012) and results in low concentrations of nitrate.

In terms of the proportion of NO_3 in NR-PM_1, the elevated NO_3 proportion in winter 2017 coincided with high NOR and high NO_2 concentrations compared to summer. The NOR in summer 2017 increased with the increase of O_x in a range of 70–130 μg m^{-3} and LWC in a range of 2.5–20 μg m^{-3}, and then decreased with much higher O_x (>130 μg m^{-3}) and LWC (>20 μg m^{-3}) (Fig. 2). As showed in Fig. S5, the increase of NO_3 concentration after 9:00 was likely caused by photochemical formation due to intensive sunlight. Note that the NO_3 concentration in winter 2017 kept increasing and reached a peak in the early night. A previous study has observed a similar increase in nitrate in the afternoon, which was linked to an increase of [Dust] × [NO_2] (Liu et al., 2020a). Thus, the possible formation pathway of nitrate was the heterogeneous reactions of NO_2 on the surface of particles which usually occurred under relatively high O_3 and medium RH.

The elevated NO_3 proportion in winter 2018 might be mainly contributed by high precursor NO_2, considering that the NOR values between the two seasons were comparable. Whereas, the elevated NO_3 proportion in winter 2020, accompanied by low NO_2, was mostly related to the efficient formation of nitrate. The NOR in the winter of 2018 and 2020 both increased with increasing O_x and increasing LWC in the whole observed ranges. The diurnal variation of NO_3 was characterized by two peaks in the morning and the early night, respectively. The dominant formation pathways of nitrate in the atmosphere include the oxidation of NO_2 by OH radicals in the gas phase, heterogeneous uptake of NO_2 on the surface of particles, and the heterogeneous reactions of N_2O_5 at night (Pandis, 2004). It's reasonably speculated that the morning peak was related to photochemical processing from precursor NO_2 and subsequent gas to particle partitioning, while the early night peak was due to the hydrolysis of N_2O_5.

3.3. Characteristics of OA factors

3.3.1. Identification and variations of OA factors

OA contributed 40.6%–52.0% to NR-PM_1 over the six observation periods in this study. To better investigate the chemical characteristics of OA, OA was identified to POA and OOA including LO-OOA and MO-OOA in this study (Fig. S2). The POA was a mixed primary OA from multiple sources. The POA mass spectrum featured strong hydrocarbon-like OA (HOA) signals, mainly $C_nH^+_{2n-1}$ (*m/z* 27, 41, 55, 69, 83, 97) and $C_nH^+_{2n+1}$ (*m/z* 29, 43, 57, 71) (Ng et al., 2011; Sun et al., 2016; Wang et al., 2016). In addition, the temporal variations of POA concentrations correlated closely with fragment ions characterizing cooking OA (COA, i.e., *m/z* 55 and *m/z* 98), biomass burning OA (BBOA, i.e., *m/z* 60 and *m/z* 73), and coal combustion OA (CCOA, i.e., *m/z* 77, *m/z* 91, and *m/z* 115). The POA profiles among the six study periods were similar, with a high correlation coefficient (r) of 0.920–0.995. OOA, usually a surrogate for SOA, has a strong signal at *m/z* 44. The OOA was classified as MO-OOA and LO-OOA according to f_{44} for each individual period. Note, the f_{44} used to divide LO-OOA and MO-OOA was not consistent among the six study periods. As shown in Fig. S3, the mass spectrometry (including f_{44} values) of MO-OOA and LO-OOA factors was very similar and could be comparable between winter and summer in the same year but significantly varied across different years.

The average contribution of POA to NR-PM_1 ranged from 8.6% to 14.0% over the six observation periods, while OOA accounted for 30.4%–38.0% of NR-PM_1. As secondary chemical components, the ratio of organic to inorganic component (i.e. OOA/SIA) had a clear increase in 2020 compared to 2017 and 2018 (Fig. 3), which reveals that SOA was increasingly important in NR-PM_1. The proportion of OOA in NR-PM_1 in the study region is comparable to those reported from Singapore (40% in 2015), India (40% in 2015), Italy (38% in 2013–2014), and western Mediterranean (38% in 2012–2013), but higher than those conducted in Shanghai (25% in 2016–2017) and Beijing (20% in 2012–2013; 30% in 2020) (Budisulistiorini et al., 2018; Bressi et al., 2016; Chakraborty et al., 2018; Hu et al., 2017; Minguillón et al., 2015; Sun et al., 2020; Zhu et al., 2021).

The diurnal variation of POA was consistent among different years and seasons, showing a distinct bimodal structure (Fig. 4a and b). The peaks appeared in the morning and evening rush hours, indicating that traffic emissions contributed significantly to POA. The result is supported by a good correlation between POA and BC that is derived mainly

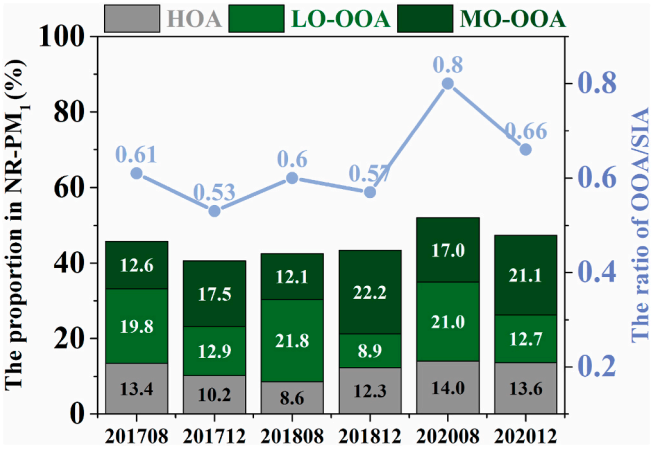

Fig. 3. The proportion of OA factors in NR-PM_1 and the ratio of OOA/SIA in six observation periods.

from traffic emissions (Fig. S8). The decrease in POA at midday and afternoon was likely due to the dynamics of the BLH. In addition, the enhanced solar radiation at midday and afternoon would promote the oxidation of POA to SOA, which also contributed to the decrease of POA.

In contrast to POA, the diurnal variation of OOA factors was significantly different between seasons. During summer, the diurnal variation of LO-OOA and MO-OOA was consistently characterized by a peak at midday (Fig. 4c, e), very similar to those of summer SO_4, which was probably caused by the enhancement of photochemical reactions due to stronger solar radiation. Differently, the peaked concentrations of MO-OOA declined more slowly than those of LO-OOA. This phenomenon has also been reported in previous studies, which was widely ascribed to the transformation of LO-OOA to MO-OOA and the contribution of long-distance transport air masses, usually with abundant MO-OOA (Cao et al., 2018; Duan et al., 2019; Li et al., 2021a; Li et al., 2021b; Zhao et al., 2017; Zhao et al., 2020). Whereas in winter, the diurnal variation of LO-OOA and MO-OOA was less consistent over the three years. One of the reasons is that the oxidation degree of the OOA factors was not comparable across the different years as mentioned above. In addition, the diurnal variation of winter OOA factors was more affected by multiple factors than a similar dominant factor. Winter is generally characterized by weak solar radiation, stable atmospheric boundary layer structure, and poor vertical diffusion of air pollutants. The diurnal variation of the OOA factors in the winters, except for winter 2018, basically showed an increase from the morning to the late afternoon, which was likely due to the synergistic effect of multiple factors, including secondary formation, transportation, and the gradual accumulation of OOA in the atmosphere (Huang et al., 2020; Li et al., 2021b; Sun et al., 2018).

3.3.2. *Oxidation degree of OA*

The f_{44} values in the component mass spectrometry reflects the absolute oxidation degree of aerosols. As shown in Fig. 5, the f_{44} of OA had a pronounced increase in 2020, indicating that the OA of 2020 was more oxidized than those of the previous two years. It is reported that the atmospheric oxidation capacity in China had increased in recent years, as the surface O_3 concentration exhibited a climbing trend (Li et al., 2021c; Qin et al., 2022). In this study, we found that the annual trend of f_{44} of OA was not corresponded to O_x concentration (Table 1). The possible reason might be the O_x concentration monitored in very short period for each individual observation campaign was largely affected by meteorological change. Long-term observations of conventional pollutants in the study region have revealed that O_x concentrations in the atmosphere substantially increased in 2020 compared to 2017 and 2018 (Fig. S9). The atmospheric oxidation capacity is also affected by other radicals, such as hydroxyl radical (OH·) and nitrate radical (NO_3·), in addition to O_x. In this study, the NO_x decreased significantly in 2020 compared to 2017 and 2018 (Table 1). It has been reported that NO_x reduction leads to the increases in oxidants (i.e. OH·, HO_2·, and NO_3·), and the increases of those oxidants in turn promote secondary aerosol formation (Huang et al., 2021; Liu et al., 2020c; Wang et al., 2021). Furthermore, many studies indicated that the gas-phase oxidation capacity increases with the decrease of aerosol concentrations, which would facilitate the conversion of precursors to secondary aerosols (Gu et al., 2020; Liu et al., 2021; Sun et al., 2020). Therefore, the increased oxidation degree of OA in 2020 could be explained by the increased

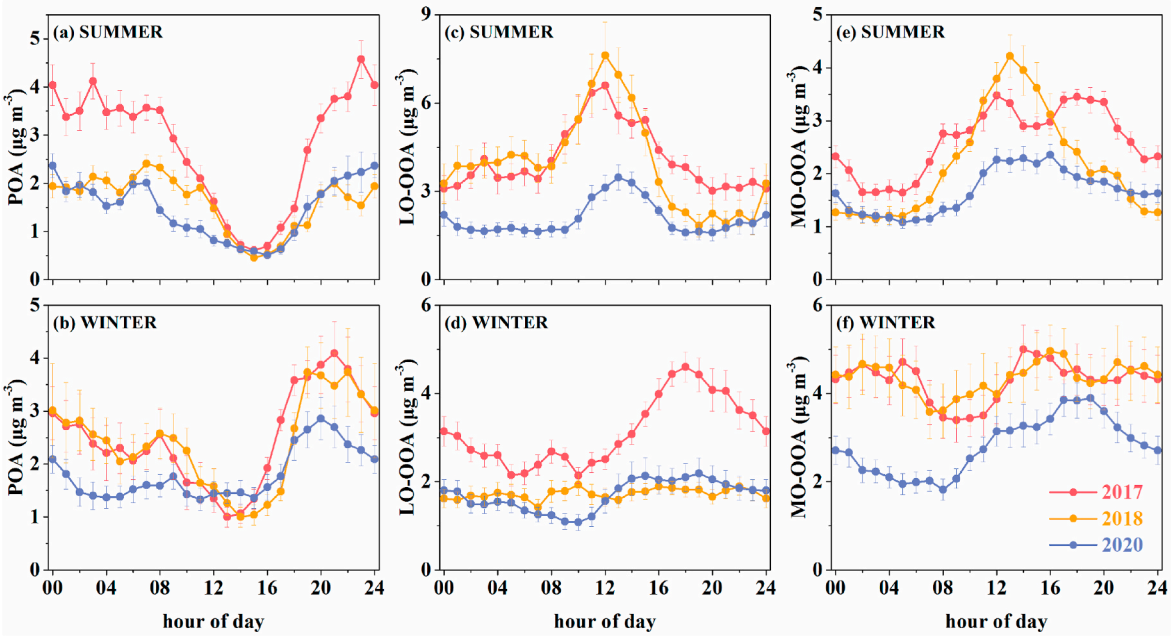

Fig. 4. Diurnal variations of POA (a, b), LO-OOA (c, d), and MO-OOA (e, f) concentrations in the summer and winter of 2017 (red), 2018 (orange), and 2020 (blue). Note: The error bar value is one-fifth of the original value. (For interpretation of the references to colour in this figure legend, the reader is referred to the Web version of this article.)

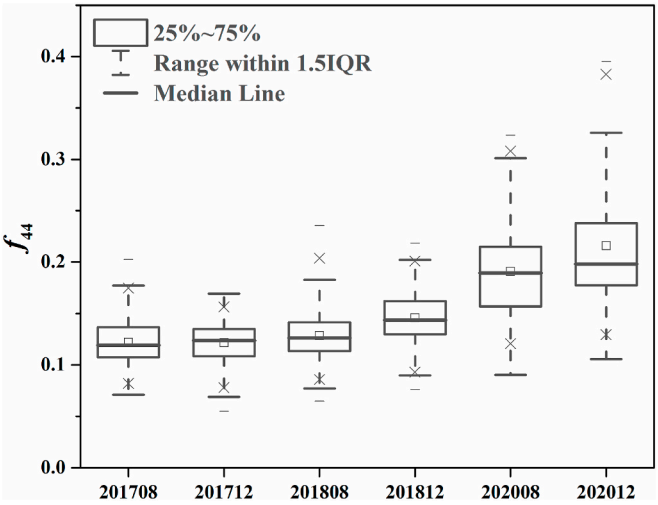

Fig. 5. The f_{44} (ratio of m/z 44 to total signal in the component MS) of OA in six observation periods.

atmospheric oxidation capacity and the decreased aerosol concentration in this year.

Additionally, long-distance transport air masses, relative to short-distance air masses, generally carry more oxidized OOA due to the extensive oxidation processes during the transport. The backward trajectory cluster results (Fig. S10) showed that the study region was significantly affected by air masses from the Philippine Sea in summer 2020 and long-distance transport air masses from Beijing-Tianjin-Hebei region and northwest China in winter 2020, compared to the corresponding periods of the other two years. Thus, it could be speculated that the more effect of long-distance transport air masses on the study region also contributed to the high oxidation degree of OA in 2020.

3.3.3. Formation mechanism of OOA

The relationships of MO-OOA/LO-OOA ratios with LWC and O_x would shed light on the formation mechanisms of OOA (Xu et al., 2017). Consistently in the summer across the different years, the variations of MO-OOA/LO-OOA ratios did not show a distinct trend with O_x, but the ratios were generally low at high O_x levels (>70 μg m^{-3}) compared to those at low O_x levels (Fig. 6d ~ f). Simultaneously, the MO-OOA/LO-OOA ratios did not increase with the increasing LWC in this study, thus aqueous phase reactions were unlikely the dominant formation pathways for MO-OOA in summer. Previous studies have reported a strong correlation between LO-OOA and VOC photochemical products and a pronounced diurnal peak of LO-OOA at midday, indicating that photochemical reactions favor the formation of LO-OOA (Chen et al., 2021; Duan et al., 2020; Hu et al., 2016; Li et al., 2018). In this study, the diurnal variation of LO-OOA and MO-OOA in summer was similarly characterized by a peak at midday (Fig. 4). Thus, we could speculate that the photochemical reactions were the main formation pathways of OOA factors in summer and it was more efficient for LO-OOA formations than for MO-OOA formations.

In contrast to summer, the variation of MO-OOA/LO-OOA ratios with LWC and O_x in winter was substantially different across the three years. The MO-OOA/LO-OOA ratios in winter 2017 slightly decreased with O_x when O_x was lower than 90 μg m^{-3} and increased with O_x when O_x exceeded 90 μg m^{-3} (Fig. 6j). Meanwhile, the ratios increased with the increasing LWC in the range of 2.5–20 μg m^{-3} (Fig. 6g). The high O_x (>90 μg m^{-3}) and moderate LWC levels (2.5–20 μg m^{-3}, corresponding RH < 80%) relating to high MO-OOA/LO-OOA ratios in winter were mostly the daytime condition (Figs. S3 and 7). As mentioned above, the diurnal variation of LO-OOA and MO-OOA in winter 2017 both increased in the morning with intensive solar radiation, which was related to photochemical reactions. Whereas, the concentrations of LO-OOA and MO-OOA peaked in the late afternoon instead of around midday. This result might be the synergistic effect of various factors, such as heterogeneous reactions under high O_x and moderate LWC conditions, transportation, and gradual accumulation. Previous studies indicated that photochemical aging would further transform LO-OOA into MO-OOA (Morgan et al., 2010; Sun et al., 2011, 2018; Via et al., 2021; Xu et al., 2017; Zhan et al., 2021). Hence, it was reasonably speculated that photochemical processing mainly contributed to LO-OOA at low O_x conditions, while at high O_x conditions, photochemical processing played a role in the transformation of LO-OOA to MO-OOA.

In winter 2018, the MO-OOA/LO-OOA ratios showed a distinct increasing trend with the increase of LWC (Fig. 6h) and the increase of O_x (Fig. 6k). The diurnal variation of LO-OOA and MO-OOA in winter 2018 was quite flat compared to other winters, which was unlike the result derived from one dominant formation pathway (Fig. 4). The result

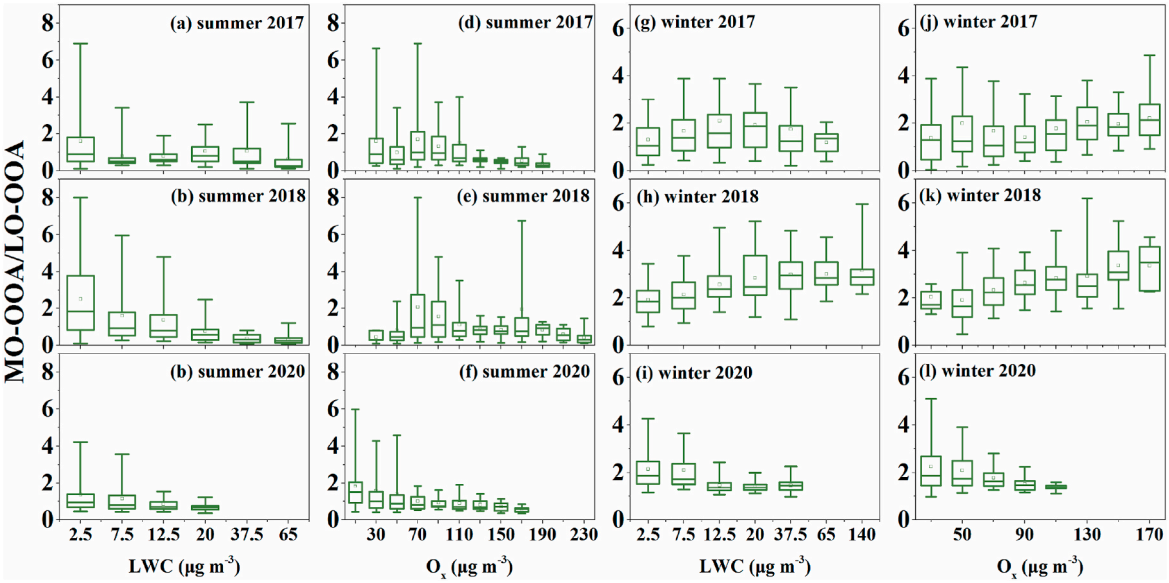

Fig. 6. Variations of MO-OOA/LO-OOA ratios as a function of LWC and O_x in summer (a ~ f) and winter (g ~ l) during 2017, 2018, and 2020. Mean (square), median (horizontal line), 25th and 75th percentiles (lower and upper box lines), and 5th and 95th percentiles (lower and upper whiskers) are displayed in the box.

suggests that both photochemistry and aqueous-phase chemistry might contribute to OOA factors and be more efficient for the formation of MO-OOA than LO-OOA in winter 2018. In addition, the high O_x in winter 2018 corresponded to a relatively low WS (Fig. S11). The low WS is not conducive to the diffusion of pollutants, which probably was beneficial to further in situ oxidation of LO-OOA and resulted in a relatively high oxidation degree of LO-OOA in this period (Fig. S2). Whereas, the MO-OOA/LO-OOA ratios in winter 2020 distinctly decreased with the increase of LWC and O_x (Fig. 6i, l), which was completely opposite to those of winter 2018. However, in terms of diurnal variations, we did not find the concentration of LO-OOA increased more remarkably than MO-OOA with the increase of LWC and O_x (Fig. 4). It could be speculated that, transportation, rather than local formation, played an important role in affecting the characteristics of OOA in winter 2020.

4. Conclusions

(1) This study investigated the chemical composition of NR-PM_1 in summer and winter of the years 2017, 2018, and 2020 in a coastal city of Southeast China. The total mass concentration of NR-PM_1 showed a decreasing trend from 2017 to 2020. The OA proportion generally increased, the NO_3 proportion decreased, and the SO_4 proportion was relatively stable among the years. The OOA contributed 30.4%–38.0% to NR-PM_1. The ratio of OOA/SIA increased in 2020, indicating that SOA was increasingly important to aerosols.

(2) The proportion of SO_4 and NO_3 in NR-PM_1 showed a significant seasonal variation. SO_4 was the dominant SIA in summer, but the contribution of NO_3 to NR-PM_1 remarkably increased and became the dominant SIA in winter. Despite the SO_2 in summer was low, the elevated SO_4 concentration in summer could be resulted from the efficient formation of SO_4, mostly via photochemical oxidation. While the high proportion of NO_3 in NR-PM_1 in winter was contributed by high precursor NO_2, and/or efficient formation of NO_3, in addition to low temperature.

(3) The oxidized degree of OA elevated from 2017 to 2020 as the f_{44} values increased. The more effect of long-distance transport air masses on the study region contributed to the high oxidation degree of OA in 2020. Photochemical reactions were the dominant pathway of OOA formation in all summers, which was more efficient for the formation of LO-OOA than MO-OOA. Whereas in winter, the diurnal variations and the main formation pathways of OOA varied across the years, which suggests the synergy of multiple factors like formation pathways and transport. The OOA in winter 2017 was mainly contributed by photochemical processing, which also played a role in the transformation of LO-OOA to MO-OOA.

CRediT authorship contribution statement

Yuping Chen: Conceptualization, Methodology, Software, Investigation, Writing – review & editing. **Chen Yang:** Conceptualization, Writing – review & editing. **Lingling Xu:** Conceptualization, Writing – review & editing. **Jinsheng Chen:** Conceptualization, Supervision, Writing – review & editing. **Yanru Zhang:** Data curation. **Jiayan Shi:** Writing – original draft. **Xiaolong Fan:** Investigation. **Ronghua Zheng:** Data curation. **Youwei Hong:** Investigation. **Mengren Li:** Investigation.

Declaration of competing interest

The authors declare that they have no known competing financial interests or personal relationships that could have appeared to influence the work reported in this paper.

Data availability

Data will be made available on request.

Acknowledgement

This study was funded by the Cultivating Project of Strategic Priority Research Program of Chinese Academy of Sciences (XDPB19003), the National Key Research and Development Program (2016YFC02005, 2016YFC0112200), the National Natural Science Foundation of China (U1405235), the Center for Excellence in Regional Atmospheric Environment, CAS (E0L1B20201), the Xiamen Youth Innovation Fund Project (3502Z20206094), State Key Laboratory of Environmental Chemistry and Ecotoxicology, Research Center for Eco-Environmental Sciences, CAS (KF2020-06), and Xiamen Atmospheric Environment Observation and Research Station of Fujian Province.

Appendix A. Supplementary data

Supplementary data to this article can be found online at https://doi.org/10.1016/j.atmosenv.2022.119243.

References

An, Z., Huang, R.J., Zhang, R., Tie, X., Li, G., Cao, J., Zhou, W., Shi, Z., Han, Y., Gu, Z., Ji, Y., 2019. Severe haze in northern China: a synergy of anthropogenic emissions and atmospheric processes. Proc. Natl. Acad. Sci. USA 116 (18), 8657–8666. https://doi.org/10.1073/pnas.1900125116.

Bressi, M., Cavalli, F., Belis, C.A., Putaud, J.P., Fröhlich, R., Martins dos Santos, S., Petralia, E., Prévôt, A.S.H., Berico, M., Malaguti, A., Canonaco, F., 2016. Variations in the chemical composition of the submicron aerosol and in the sources of the organic fraction at a regional background site of the Po Valley (Italy). Atmos. Chem. Phys. 16, 12875–12896. https://doi.org/10.5194/acp-16-12875-2016.

Brito, J., Rizzo, L.V., Morgan, W.T., Coe, H., Johnson, B., Haywood, J., Longo, K., Freitas, S., Andreae, M.O., Artaxo, P., 2014. Ground-based aerosol characterization during the south American biomass burning analysis (SAMBBA) field experiment. Atmos. Chem. Phys. 14 (22), 12069–12083. https://doi.org/10.5194/acp-14-12069-2014.

Budisulistiorini, S.H., Riva, M., Williams, M., Miyakawa, T., Chen, J., Itoh, M., Surratt, J. D., Kuwata, M., 2018. Dominant contribution of oxygenated organic aerosol to haze particles from real-time observation in Singapore during an Indonesian wildfire event in 2015. Atmos. Chem. Phys. 18 (22), 16481–16498. https://doi.org/10.5194/acp-18-16481-2018.

Canagaratna, M.R., Jayne, J.T., Jimenez, J.L., Allan, J.D., Alfarra, M.R., Zhang, Q., Onasch, T.B., Drewnick, F., Coe, H., Middlebrook, A., Delia, A., Williams, L.R., Trimborn, A.M., Northway, M.J., DeCarlo, P.F., Kolb, C.E., Davidovits, P., Worsnop, D.R., 2007. Chemical and microphysical characterization of ambient aerosols with the aerodyne aerosol mass spectrometer. Mass Spectrom. Rev. 26 (2), 185–222. https://doi.org/10.1002/mas.20115.

Canonaco, F., Crippa, M., Slowik, J.G., Baltensperger, U., Prévôt, A.S.H., 2013. SoFi, an IGOR-based interface for the efficient use of the generalized multilinear engine (ME-2) for the source apportionment: ME-2 application to aerosol mass spectrometer data. Atmos. Meas. Tech. 6 (12), 3649–3661. https://doi.org/10.5194/amt-6-3649-2013.

Cao, L.M., Huang, X.F., Li, Y.Y., Hu, M., He, L.Y., 2018. Volatility measurement of atmospheric submicron aerosols in an urban atmosphere in southern China. Atmos. Chem. Phys. 18 (3), 1729–1743. https://doi.org/10.5194/acp-18-1729-2018.

Chakraborty, A., Mandariya, A.K., Chakraborti, R., Gupta, T., Tripathi, S.N., 2018. Realtime chemical characterization of post monsoon organic aerosols in a polluted urban city: sources, composition, and comparison with other seasons. Environ. Pollut. 232, 310–321. https://doi.org/10.1016/j.envpol.2017.09.079.

Chazeau, B., Temime-Roussel, B., Gille, G., Mesbah, B., D'Anna, B., Wortham, H., Marchand, N., 2021. Measurement report: fourteen months of real-time characterisation of the submicronic aerosol and its atmospheric dynamics at the Marseille–Longchamp supersite. Atmos. Chem. Phys. 21 (9), 7293–7319. https://doi.org/10.5194/acp-21-7293-2021.

Chen, T., Liu, J., Ma, Q., Chu, B., Zhang, P., Ma, J., Liu, Y., Zhong, C., Liu, P., Wang, Y., Mu, Y., He, H., 2021. Measurement report: effects of photochemical aging on the formation and evolution of summertime secondary aerosol in Beijing. Atmos. Chem. Phys. 21 (2), 1341–1356. https://doi.org/10.5194/acp-21-1341-2021.

Cheng, Y.F., Zheng, G.J., Wei, C., Mu, Q., Zheng, B., Wang, Z.B., Gao, M., Zhang, Q., He, K.B., Carmichael, G., Poschl, U., Su, H., 2016. Reactive nitrogen chemistry in aerosol water as a source of sulfate during haze events in China. Sci. Adv. 2 (12) https://doi.org/10.1126/sciadv.1601530.

Dai, Q., Schulze, B.C., Bi, X., Bui, A.A.T., Guo, F., Wallace, H.W., Sanchez, N.P., Flynn, J. H., Lefer, B.L., Feng, Y., Griffin, R.J., 2019. Seasonal differences in formation processes of oxidized organic aerosol near Houston, TX. Atmos. Chem. Phys. 19 (14), 9641–9661. https://doi.org/10.5194/acp-19-9641-2019.

Duan, J., Huang, R.-J., Lin, C., Dai, W., Wang, M., Gu, Y., Wang, Y., Zhong, H., Zheng, Y., Ni, H., Dusek, U., Chen, Y., Li, Y., Chen, Q., Worsnop, D.R., O'Dowd, C.D., Cao, J., 2019. Distinctions in source regions and formation mechanisms of secondary aerosol in Beijing from summer to winter. Atmos. Chem. Phys. 19 (15), 10319–10334. https://doi.org/10.5194/acp-19-10319-2019.

Duan, J., Huang, R.-J., Li, Y., Chen, Q., Zheng, Y., Chen, Y., Lin, C., Ni, H., Wang, M., Ovadnevaite, J., Ceburnis, D., Chen, C., Worsnop, D.R., Hoffmann, T., O'Dowd, C., Cao, J., 2020. Summertime and wintertime atmospheric processes of secondary aerosol in Beijing. Atmos. Chem. Phys. 20 (6), 3793–3807. https://doi.org/10.5194/acp-20-3793-2020.

Fountoukis, C., Nenes, A., 2007. Isotropic II: a computationally efficient thermodynamic equilibrium model for K^+–Ca^{2+}–Mg^{2+}–NH_4^+–Na^+–SO_4^{2-}–NO_3^-–Cl^-–H_2O aerosols. Atmos. Chem. Phys. 7, 4639–4659. https://doi.org/10.5194/acp-7-4639-2007.

Fröhlich, R., Crenn, V., Setyan, A., Belis, C.A., Canonaco, F., Favez, O., Riffault, V., Slowik, J.G., Aas, W., Aijälä, M., Alastuey, A., Artiñano, B., Bonnaire, N., Bozzetti, C., Bressi, M., Carbone, C., Coz, E., Croteau, P.L., Cubison, M.J., Esser-Gietl, J.K., Green, D.C., Gros, V., Heikkinen, L., Herrmann, H., Jayne, J.T., Lunder, C.R., Minguillón, M.C., Močnik, G., O'Dowd, C.D., Ovadnevaite, J., Petralia, E., Poulain, L., Priestman, M., Ripoll, A., Sarda-Estève, R., Wiedensohler, A., Baltensperger, U., Sciare, J., Prévôt, A.S.H., 2015. ACTRIS ACSM intercomparison – Part 2: intercomparison of ME-2 organic source apportionment results from 15 individual, co-located aerosol mass spectrometers. Atmos. Meas. Tech. 8 (6), 2555–2576. https://doi.org/10.5194/amt-8-2555-2015.

Gu, Y., Huang, R.J., Li, Y., Duan, J., Chen, Q., Hu, W., Zheng, Y., Lin, C., Ni, H., Dai, W., Cao, J., Liu, Q., Chen, Y., Chen, C., Ovadnevaite, J., Ceburnis, D., O'Dowd, C., 2020. Chemical nature and sources of fine particles in urban Beijing: seasonality and formation mechanisms. Environ. Int. 140, 105732 https://doi.org/10.1016/j.envint.2020.105732.

Guo, J., Zhou, S., Cai, M., Zhao, J., Song, W., Zhao, W., Hu, W., Sun, Y., He, Y., Yang, C., Xu, X., Zhang, Z., Cheng, P., Fan, Q., Hang, J., Fan, S., Wang, X., Wang, X., 2020. Characterization of submicron particles by time-of-flight aerosol chemical speciation monitor (ToF-ACSM) during wintertime: aerosol composition, sources, and chemical processes in Guangzhou, China. Atmos. Chem. Phys. 20 (12), 7595–7615. https://doi.org/10.5194/acp-20-7595-2020.

Gunthe, S.S., Rose, D., Su, H., Garland, R.M., Achtert, P., Nowak, A., Wiedensohler, A., Kuwata, M., Takegawa, N., Kondo, Y., Hu, M., Shao, M., Zhu, T., Andreae, M.O., Pöschl, U., 2011. Cloud condensation nuclei (CCN) from fresh and aged air pollution in the megacity region of Beijing. Atmos. Chem. Phys. 11, 11023–11039. https://doi.org/10.5194/acp-11-11023-2011.

Hallquist, M., Wenger, J.C., Baltensperger, U., Rudich, Y., Simpson, D., Claeys, M., Dommen, J., Donahue, N.M., George, C., Goldstein, A.H., Hamilton, J.F., Herrmann, H., Hoffmann, T., Iinuma, Y., Jang, M., Jenkin, M.E., Jimenez, J.L., Kiendler-Scharr, A., Maenhaut, W., McFiggans, G., Mentel, T.F., Monod, A., Prevot, A.S.H., Seinfeld, J.H., Surratt, J.D., Szmigielski, R., Wildt, J., 2009. The formation, properties and impact of secondary organic aerosol: current and emerging issues. Atmos. Chem. Phys. 9 (14), 5155–5236. https://doi.org/10.5194/acp-9-5155-2009.

Harris, E., Sinha, B., van Pinxteren, D., Tilgner, A., Fomba, K.W., Schneider, J., Roth, A., Gnauk, T., Fahlbusch, B., Mertes, S., Lee, T., Collett, J., Foley, S., Borrmann, S., Hoppe, P., Herrmann, H., 2013. Enhanced role of transition metal ion catalysis during in-cloud oxidation of SO_2. Science 340 (6133), 727–730. https://doi.org/10.1126/science.1230911.

Heal, M.R., Kumar, P., Harrison, R.M., 2012. Particles, air quality, policy and health. Chem. Soc. Rev. 41 (19), 6606–6630. https://doi.org/10.1039/c2cs35076a.

Hu, W., Hu, M., Hu, W., Jimenez, J.L., Yuan, B., Chen, W., Wang, M., Wu, Y., Chen, C., Wang, Z., Peng, J., Zeng, L., Shao, M., 2016. Chemical composition, sources, and aging process of submicron aerosols in Beijing: contrast between summer and winter. J. Geophys. Res. Atmos. 121 (4), 1955–1977. https://doi.org/10.1002/2015jd024020.

Hu, W., Hu, M., Hu, W.-W., Zheng, J., Chen, C., Wu, Y., Guo, S., 2017. Seasonal variations in high time-resolved chemical compositions, sources, and evolution of atmospheric submicron aerosols in the megacity Beijing. Atmos. Chem. Phys. 17 (16), 9979–10000. https://doi.org/10.5194/acp-17-9979-2017.

Huang, R.J., Zhang, Y., Bozzetti, C., Ho, K.F., Cao, J.J., Han, Y., Daellenbach, K.R., Slowik, J.G., Platt, S.M., Canonaco, F., Zotter, P., Wolf, R., Pieber, S.M., Bruns, E.A., Crippa, M., Ciarelli, G., Piazzalunga, A., Schwikowski, M., Abbaszade, G., Schnelle-Kreis, J., Zimmermann, R., An, Z., Szidat, S., Baltensperger, U., El Haddad, I., Prevot, A.S., 2014. High secondary aerosol contribution to particulate pollution during haze events in China. Nature 514 (7521), 218–222. https://doi.org/10.1038/nature13774.

Huang, R.J., He, Y., Duan, J., Li, Y., Chen, Q., Zheng, Y., Chen, Y., Hu, W., Lin, C., Ni, H., Dai, W., Cao, J., Wu, Y., Zhang, R., Xu, W., Ovadnevaite, J., Ceburnis, D., Hoffmann, T., O'Dowd, C.D., 2020. Contrasting sources and processes of particulate species in haze days with low and high relative humidity in wintertime Beijing. Atmos. Chem. Phys. 20 (14), 9101–9114. https://doi.org/10.5194/acp-20-9101-2020.

Huang, X., Ding, A., Gao, J., Zheng, B., Zhou, D., Qi, X., Tang, R., Wang, J., Ren, C., Nie, W., Chi, X., Xu, Z., Chen, L., Li, Y., Che, F., Pang, N., Wang, H., Tong, D., Qin, W., Cheng, W., Liu, W., Fu, Q., Liu, B., Chai, F., Davis, S.J., Zhang, Q., He, K., 2021. Enhanced secondary pollution offset reduction of primary emissions during COVID-19 lockdown in China. Natl. Sci. Rev. 8 (2), nwaa137. https://doi.org/10.1093/nsr/nwaa137.

IPCC, Intergovernmental Panel on Climate Change, 2021. Climate Change 2021: the Physical Science Basis. Cambridge University Press, Cambridge.

Jimenez, J.L., Canagaratna, M.R., Donahue, N.M., Prevot, A.S., Zhang, Q., Kroll, J.H., DeCarlo, P.F., Allan, J.D., Coe, H., Ng, N.L., Aiken, A.C., Docherty, K.S., Ulbrich, I. M., Grieshop, A.P., Robinson, A.L., Duplissy, J., Smith, J.D., Wilson, K.R., Lanz, V.A., Hueglin, C., Sun, Y.L., Tian, J., Laaksonen, A., Raatikainen, T., Rautiainen, J., Vaattovaara, P., Ehn, M., Kulmala, M., Tomlinson, J.M., Collins, D.R., Cubison, M.J., Dunlea, E.J., Huffman, J.A., Onasch, T.B., Alfarra, M.R., Williams, P.I., Bower, K., Kondo, Y., Schneider, J., Drewnick, F., Borrmann, S., Weimer, S., Demerjian, K., Salcedo, D., Cottrell, L., Griffin, R., Takami, A., Miyoshi, T., Hatakeyama, S., Shimono, A., Sun, J.Y., Zhang, Y.M., Dzepina, K., Kimmel, J.R., Sueper, D., Jayne, J. T., Herndon, S.C., Trimborn, A.M., Williams, L.R., Wood, E.C., Middlebrook, A.M., Kolb, C.E., Baltensperger, U., Worsnop, D.R., 2009. Evolution of organic aerosols in the atmosphere. Science 326 (5959), 1525–1529. https://doi.org/10.1126/science.1180353.

Kreyling, W.G., Semmler-Behnke, M., Möller, W., 2006. Health implications of nanoparticles. J. Nanoparticle Res. 8 (5), 543–562. https://doi.org/10.1007/s11051-005-9068-z.

Kroll, J.H., Seinfeld, J.H., 2008. Chemistry of secondary organic aerosol: formation and evolution of low-volatility organics in the atmosphere. Atmos. Environ. 42 (16), 3593–3624. https://doi.org/10.1016/j.atmosenv.2008.01.003.

Kuwata, M., Zorn, S.R., Martin, S.T., 2011. Using elemental ratios to predict the density of organic material composed of carbon, hydrogen, and oxygen. Environ. Sci. Technol. 46 (2), 787–794. https://doi.org/10.1021/es202525q.

Lei, L., Zhou, W., Chen, C., He, Y., Li, Z., Sun, J., Tang, X., Fu, P., Wang, Z., Sun, Y., 2021. Long-term characterization of aerosol chemistry in cold season from 2013 to 2020 in Beijing, China. Environ. Pollut. 268, 115952 https://doi.org/10.1016/j.envpol.2020.115952.

Li, G., Bei, N., Cao, J., Huang, R., Wu, J., Feng, T., Wang, Y., Liu, S., Zhang, Q., Tie, X., Molina, L.T., 2017b. A possible pathway for rapid growth of sulfate during haze days in China. Atmos. Chem. Phys. 17 (5), 3301–3316. https://doi.org/10.5194/acp-17-3301-2017.

Li, J., Cao, L., Gao, W., He, L., Yan, Y., He, Y., Pan, Y., Ji, D., Liu, Z., Wang, Y., 2021b. Seasonal variations in the highly time-resolved aerosol composition, sources and chemical processes of background submicron particles in the North China Plain. Atmos. Chem. Phys. 21 (6), 4521–4539. https://doi.org/10.5194/acp-21-4521-2021.

Li, J., Gao, W., Cao, L., Xiao, Y., Zhang, Y., Zhao, S., Liu, Z., Liu, Z., Tang, G., Ji, D., Hu, B., Song, T., He, L., Hu, M., Wang, Y., 2021a. Significant changes in autumn and winter aerosol composition and sources in Beijing from 2012 to 2018: effects of clean air actions. Environ. Pollut. 268, 115855 https://doi.org/10.1016/j.envpol.2020.115855.

Li, K., Chen, L., White, S.J., Zheng, X., Lv, B., Lin, C., Bao, Z., Wu, X., Gao, X., Ying, F., Shen, J., Azzi, M., Cen, K., 2018. Chemical characteristics and sources of PM_1 during the 2016 summer in Hangzhou. Environ. Pollut. 232, 42–54. https://doi.org/10.1016/j.envpol.2017.09.016.

Li, K., Jacob, D.J., Liao, H., Qiu, Y., Shen, L., Zhai, S., Bates, K.H., Sulprizio, M.P., Song, S., Lu, X., Zhang, Q., Zheng, B., Zhang, Y., Zhang, J., Lee, H.C., Kuk, S.K., 2021c. Ozone pollution in the North China Plain spreading into the late-winter haze season. Proc. Natl. Acad. Sci. U. S. A. 118 (10) https://doi.org/10.1073/pnas.2015797118.

Li, Y.J., Sun, Y., Zhang, Q., Li, X., Li, M., Zhou, Z., Chan, C.K., 2017a. Real-time chemical characterization of atmospheric particulate matter in China: a review. Atmos. Environ. 158, 270–304. https://doi.org/10.1016/j.atmosenv.2017.02.027.

Liu, J., Chu, B., Chen, T., Zhong, C., Liu, C., Ma, Q., Ma, J., Zhang, P., He, H., 2021. Secondary organic aerosol formation potential from ambient air in beijing: effects of atmospheric oxidation capacity at different pollution levels. Environ. Sci. Technol. 55 (8), 4565–4572. https://doi.org/10.1021/acs.est.1c00890.

Liu, P., Ye, C., Xue, C., Zhang, C., Mu, Y., Sun, X., 2020a. Formation mechanisms of atmospheric nitrate and sulfate during the winter haze pollution periods in Beijing: gas-phase, heterogeneous and aqueous-phase chemistry. Atmos. Chem. Phys. 20 (7), 4153–4165. https://doi.org/10.5194/acp-20-4153-2020.

Liu, T., Clegg, S.L., Abbatt, J.P.D., 2020b. Fast oxidation of sulfur dioxide by hydrogen peroxide in deliquesced aerosol particles. Proc. Natl. Acad. Sci. USA 117 (3), 1354–1359. https://doi.org/10.1073/pnas.1916401117.

Liu, T., Wang, X., Hu, J., Wang, Q., An, J., Gong, K., Sun, J., Li, L., Qin, M., Li, J., Tian, J., Huang, Y., Liao, H., Zhou, M., Hu, Q., Yan, R., Wang, H., Huang, C.: Driving forces of changes in air quality during the COVID-19 lockdown period in the Yangtze River Delta region, China. Environ. Sci. Technol. Lett. 7 (11), 779-786. doi:10.1021/acs.estlett.0c00511,2020c.

Meng, Z.Y., Lin, W.L., Jiang, X.M., Yan, P., Wang, Y., Zhang, Y.M., Jia, X.F., Yu, X.L., 2011. Characteristics of atmospheric ammonia over Beijing, China. Atmos. Chem. Phys. 11 (12), 6139–6151. https://doi.org/10.5194/acp-11-6139-2011.

Mei, F., Setyan, A., Zhang, Q., Wang, J., 2013. CCN activity of organic aerosols observed downwind of urban emissions during CARES. Atmos. Chem. Phys. 13 (24), 12155–12169. https://doi.org/10.5194/acp-13-12155-2013.

Middlebrook, A.M., Bahreini, R., Jimenez, J.L., Canagaratna, M.R., 2012. Evaluation of composition-dependent collection efficiencies for the aerodyne aerosol mass spectrometer using field data. Aerosol Sci. Technol. 46 (3), 258–271. https://doi.org/10.1080/02786826.2011.620041.

Minguillón, M.C., Ripoll, A., Pérez, N., Prévôt, A.S.H., Canonaco, F., Querol, X., Alastuey, A., 2015. Chemical characterization of submicron regional background aerosols in the western Mediterranean using an Aerosol Chemical Speciation Monitor. Atmos. Chem. Phys. 15 (11), 6379–6391. https://doi.org/10.5194/acp-15-6379-2015.

Morgan, W.T., Allan, J.D., Bower, K.N., Highwood, E.J., Liu, D., McMeeking, G.R., Northway, M.J., Williams, P.I., Krejci, R., Coe, H., 2010. Airborne measurements of the spatial distribution of aerosol chemical composition across Europe and evolution of the organic fraction. Atmos. Chem. Phys. 10 (8), 4065–4083. https://doi.org/10.5194/acp-10-4065-2010.

Ng, N.L., Herndon, S.C., Trimborn, A., Canagaratna, M.R., Croteau, P.L., Onasch, T.B., Sueper, D., Worsnop, D.R., Zhang, Q., Sun, Y.L., Jayne, J.T., 2011. An aerosol chemical speciation monitor (ACSM) for routine monitoring of the composition and mass concentrations of ambient aerosol. Aerosol Sci. Technol. 45 (7), 780–794. https://doi.org/10.1080/02786826.2011.560211.

Paatero, P., Tapper, U., 1994. Positive matrix factorization: a non-negative factor model with optimal utilization of error estimates of data values. Environmetrics 5, 111–126.

Pandis, S., 2004. In: McMurry, P., Shepherd, M., Vickery, J. (Eds.), Atmospheric Aerosol Processes. Particulate Matter Assessment for Policy Makers: a NARSTO Assessment.. Cambridge University Press, Cambridge, England.

Petters, M.D., Kreidenweis, S.M., 2007. A single parameter representation of hygroscopic growth and cloud condensation nucleus activity. Atmos. Chem. Phys. 7 (8), 1961–1971. https://doi.org/10.5194/acp-7-1961-2007.

Pieber, S.M., El Haddad, I., Slowik, J.G., Canagaratna, M.R., Jayne, J.T., Platt, S.M., Bozzetti, C., Daellenbach, K.R., Frohlich, R., Vlachou, A., Klein, F., Dommen, J., Miljevic, B., Jimenez, J.L., Worsnop, D.R., Baltensperger, U., Prevot, A.S., 2016. Inorganic salt interference on CO_2^+ in aerodyne AMS and ACSM organic aerosol composition studies. Environ. Sci. Technol. 50 (19), 10494–10503. https://doi.org/10.1021/acs.est.6b01035.

Pöschl, U., 2005. Atmospheric aerosols: composition, transformation, climate and health effects. Angew. Chem., Int. Ed. Engl. 44 (46), 7520–7540. https://doi.org/10.1002/anie.200501122.

Qin, M., Hu, A., Mao, J., Li, X., Sheng, L., Sun, J., Li, J., Wang, X., Zhang, Y., Hu, J., 2022. $PM_{2.5}$ and O_3 relationships affected by the atmospheric oxidizing capacity in the Yangtze River Delta, China. Sci. Total Environ. 810, 152268 https://doi.org/10.1016/j.scitotenv.2021.152268.

Seinfeld, J.H., Pandis, S.N., 2016. Atmospheric Chemistry and Physics: from Air Pollution to Climate Change. John Wiley & Sons, New York.

Sun, Y.L., Zhang, Q., Schwab, J.J., Chen, W.N., Bae, M.S., Lin, Y.C., Hung, H.M., Demerjian, K.L., 2011. A case study of aerosol processing and evolution in summer in New York City. Atmos. Chem. Phys. 11 (24), 12737–12750. https://doi.org/10.5194/acp-11-12737-2011.

Sun, Y., Wang, Z., Dong, H., Yang, T., Li, J., Pan, X., Chen, P., Jayne, J.T., 2012. Characterization of summer organic and inorganic aerosols in beijing, China with an aerosol chemical speciation monitor. Atmos. Environ. 51, 250–259. https://doi.org/10.1016/j.atmosenv.2012.01.013.

Sun, Y., Jiang, Q., Wang, Z., Fu, P., Li, J., Yang, T., Yin, Y., 2014. Investigation of the sources and evolution processes of severe haze pollution in Beijing in January 2013. J. Geophys. Res. Atmos. 119 (7), 4380–4398. https://doi.org/10.1002/2014jd021641.

Sun, Y., Du, W., Wang, Q., Zhang, Q., Chen, C., Chen, Y., Chen, Z., Fu, P., Wang, Z., Gao, Z., Worsnop, D.R., 2015. Real-time characterization of aerosol particle composition above the urban canopy in beijing: insights into the interactions between the atmospheric boundary layer and aerosol chemistry. Environ. Sci. Technol. 49 (19), 11340–11347. https://doi.org/10.1021/acs.est.5b02373.

Sun, Y., Du, W., Fu, P., Wang, Q., Li, J., Ge, X., Zhang, Q., Zhu, C., Ren, L., Xu, W., Zhao, J., Han, T., Worsnop, D.R., Wang, Z., 2016. Primary and secondary aerosols in Beijing in winter: sources, variations and processes. Atmos. Chem. Phys. 16 (13), 8309–8329. https://doi.org/10.5194/acp-16-8309-2016.

Sun, Y., Xu, W., Zhang, Q., Jiang, Q., Canonaco, F., Prévôt, A.S.H., Fu, P., Li, J., Jayne, J., Worsnop, D.R., Wang, Z., 2018. Source apportionment of organic aerosol from 2-year highly time-resolved measurements by an aerosol chemical speciation monitor in Beijing, China. Atmos. Chem. Phys. 18 (12), 8469–8489. https://doi.org/10.5194/acp-18-8469-2018.

Sun, Y., Lei, L., Zhou, W., Chen, C., He, Y., Sun, J., Li, Z., Xu, W., Wang, Q., Ji, D., Fu, P., Wang, Z., Worsnop, D.R., 2020. A chemical cocktail during the COVID-19 outbreak in Beijing, China: insights from six-year aerosol particle composition measurements during the Chinese New Year holiday. Sci. Total Environ. 742, 140739 https://doi.org/10.1016/j.scitotenv.2020.140739.

Tiitta, P., Vakkari, V., Croteau, P., Beukes, J.P., van Zyl, P.G., Josipovic, M., Venter, A.D., Jaars, K., Pienaar, J.J., Ng, N.L., Canagaratna, M.R., Jayne, J.T., Kerminen, V.M., Kokkola, H., Kulmala, M., Laaksonen, A., Worsnop, D.R., Laakso, L., 2014. Chemical composition, main sources and temporal variability of PM_1 aerosols in southern African grassland. Atmos. Chem. Phys. 14 (4), 1909–1927. https://doi.org/10.5194/acp-14-1909-2014.

Tobler, A.K., Skiba, A., Wang, D.S., Croteau, P., Styszko, K., Nęcki, J., Baltensperger, U., Slowik, J.G., Prévôt, A.S.H., 2020. Improved chloride quantification in quadrupole aerosol chemical speciation monitors (Q-ACSMs). Atmos. Meas. Tech. 13 (10), 5293–5301. https://doi.org/10.5194/amt-13-5293-2020.

Tobler, A.K., Skiba, A., Canonaco, F., Močnik, G., Rai, P., Chen, G., Bartyzel, J., Zimnoch, M., Styszko, K., Nęcki, J., Furger, M., Różański, K., Baltensperger, U., Slowik, J.G., Prevot, A.S.H., 2021. Characterization of non-refractory (NR) PM_1 and source apportionment of organic aerosol in Kraków, Poland. Atmos. Chem. Phys. 21 (19), 14893–14906. https://doi.org/10.5194/acp-21-14893-2021.

Ulbrich, I.M., Canagaratna, M.R., Zhang, Q., Worsnop, D.R., Jimenez, J.L., 2009. Interpretation of organic components from Positive Matrix Factorization of aerosol mass spectrometric data. Atmos. Chem. Phys. 9 (9), 2891–2918. https://doi.org/10.5194/acp-9-2891-2009.

Via, M., Minguillón, M.C., Reche, C., Querol, X., Alastuey, A., 2021. Increase in secondary organic aerosol in an urban environment. Atmos. Chem. Phys. 21 (10), 8323–8339. https://doi.org/10.5194/acp-21-8323-2021.

Wang, J., Li, J., Ye, J., Zhao, J., Wu, Y., Hu, J., Liu, D., Nie, D., Shen, F., Huang, X., Huang, D.D., Ji, D., Sun, X., Xu, W., Guo, J., Song, S., Qin, Y., Liu, P., Turner, J.R., Lee, H.C., Hwang, S., Liao, H., Martin, S.T., Zhang, Q., Chen, M., Sun, Y., Ge, X., Jacob, D.J., 2020. Fast sulfate formation from oxidation of SO_2 by NO_2 and HONO observed in Beijing haze. Nat. Commun. 11 (1), 2844. https://doi.org/10.1038/s41467-020-16683-x.

Wang, Q., Zhao, J., Du, W., Ana, G., Wang, Z., Sun, L., Wang, Y., Zhang, F., Li, Z., Ye, X., Sun, Y., 2016. Characterization of submicron aerosols at a suburban site in central China. Atmos. Environ. 131, 115–123. https://doi.org/10.1016/j.atmosenv.2016.01.054.

Wang, Y., Zhang, Q., Jiang, J., Zhou, W., Wang, B., He, K., Duan, F., Zhang, Q., Philip, S., Xie, Y., 2014. Enhanced sulfate formation during China's severe winter haze episode in January 2013 missing from current models. J. Geophys. Res. Atmos. 119 (17), 10. https://doi.org/10.1002/2013jd021426, 425-10,440.

Wang, Y.C., Huang, R.J., Ni, H.Y., Chen, Y., Wang, Q.Y., Li, G.H., Tie, X.X., Shen, Z.X., Huang, Y., Liu, S.X., Dong, W.M., Xue, P., Fröhlich, R., Canonaco, F., Elser, M., Daellenbach, K.R., Bozzetti, C., El Haddad, I., Prévôt, A.S.H., Canagaratna, M.R., Worsnop, D.R., Cao, J.J., 2017. Chemical composition, sources and secondary processes of aerosols in Baoji city of northwest China. Atmos. Environ. 158, 128–137. https://doi.org/10.1016/j.atmosenv.2017.03.026.

Wang, Y., Zhu, S., Ma, J., Shen, J., Wang, P., Wang, P., Zhang, H., 2021. Enhanced atmospheric oxidation capacity and associated ozone increases during COVID-19 lockdown in the Yangtze River Delta. Sci. Total Environ. 768, 144796 https://doi.org/10.1016/j.scitotenv.2020.144796.

Xiao, Y., Hu, M., Zong, T., Wu, Z., Tan, T., Zhang, Z., Fang, X., Chen, S., Guo, S., 2021. Insights into aqueous-phase and photochemical formation of secondary organic aerosol in the winter of Beijing. Atmos. Environ. 259 https://doi.org/10.1016/j.atmosenv.2021.118535.

Xu, J., Zhang, Q., Chen, M., Ge, X., Ren, J., Qin, D., 2014. Chemical composition, sources, and processes of urban aerosols during summertime in northwest China: insights from high-resolution aerosol mass spectrometry. Atmos. Chem. Phys. 14 (23), 12593–12611. https://doi.org/10.5194/acp-14-12593-2014.

Xu, Q., Wang, S., Jiang, J., Bhattarai, N., Li, X., Chang, X., Qiu, X., Zheng, M., Hua, Y., Hao, J., 2019. Nitrate dominates the chemical composition of $PM_{2.5}$ during haze event in Beijing, China. Sci. Total Environ. 689, 1293–1303. https://doi.org/10.1016/j.scitotenv.2019.06.294.

Xu, W., Han, T., Du, W., Wang, Q., Chen, C., Zhao, J., Zhang, Y., Li, J., Fu, P., Wang, Z., Worsnop, D.R., Sun, Y., 2017. Effects of aqueous-phase and photochemical processing on secondary organic aerosol formation and evolution in Beijing, China. Environ. Sci. Technol. 51 (2), 762–770. https://doi.org/10.1021/acs.est.6b04498.

Xu, W.Q., Sun, Y.L., Chen, C., Du, W., Han, T.T., Wang, Q.Q., Fu, P.Q., Wang, Z.F., Zhao, X.J., Zhou, L.B., Ji, D.S., Wang, P.C., Worsnop, D.R., 2015. Aerosol composition, oxidation properties, and sources in Beijing: results from the 2014 Asia-Pacific Economic Cooperation summit study. Atmos. Chem. Phys. 15 (23), 13681–13698. https://doi.org/10.5194/acp-15-13681-2015.

Yang, H., Wang, J., Chen, M., Nie, D., Shen, F., Lei, Y., Ge, P., Gu, T., Gai, X., Huang, X., Ma, Q., 2020. Chemical characteristics, sources and evolution processes of fine particles in Lin'an, Yangtze River Delta, China. Chemosphere 254, 126851. https://doi.org/10.1016/j.chemosphere.2020.126851.

Yang, S., Liu, Z., Li, J., Zhao, S., Xu, Z., Gao, W., Hu, B., Wang, Y., 2021. Insights into the chemistry of aerosol growth in Beijing: implication of fine particle episode formation during wintertime. Chemosphere 274, 129776. https://doi.org/10.1016/j.chemosphere.2021.129776.

Zhan, B., Zhong, H., Chen, H., Chen, Y., Li, X., Wang, L., Wang, X., Mu, Y., Huang, R.-J., George, C., Chen, J., 2021. The roles of aqueous-phase chemistry and photochemical oxidation in oxygenated organic aerosols formation. Atmos. Environ. 266 https://doi.org/10.1016/j.atmosenv.2021.118738.

Zhang, Y., Xu, L., Zhuang, M., Zhao, G., Chen, Y., Tong, L., Yang, C., Xiao, H., Chen, J., Wu, X., Hong, Y., Li, M., Bian, Y., Chen, Y., 2020. Chemical composition and sources of submicron aerosol in a coastal city of China: results from the 2017 BRICS summit study. Sci. Total Environ. 741, 140470 https://doi.org/10.1016/j.scitotenv.2020.140470.

Zhao, J., Du, W., Zhang, Y., Wang, Q., Chen, C., Xu, W., Han, T., Wang, Y., Fu, P., Wang, Z., Li, Z., Sun, Y., 2017. Insights into aerosol chemistry during the 2015 China Victory Day parade: results from simultaneous measurements at ground level and 260 m in Beijing. Atmos. Chem. Phys. 17 (4), 3215–3232. https://doi.org/10.5194/acp-17-3215-2017.

Zhao, Q., Huo, J., Yang, X., Fu, Q., Duan, Y., Liu, Y., Lin, Y., Zhang, Q., 2020. Chemical characterization and source identification of submicron aerosols from a year-long real-time observation at a rural site of Shanghai using an Aerosol Chemical Speciation Monitor. Atmos. Res. 246 https://doi.org/10.1016/j.atmosres.2020.105154.

Zheng, G.J., Duan, F.K., Su, H., Ma, Y.L., Cheng, Y., Zheng, B., Zhang, Q., Huang, T., Kimoto, T., Chang, D., Pöschl, U., Cheng, Y.F., He, K.B., 2015. Exploring the severe winter haze in Beijing: the impact of synoptic weather, regional transport and heterogeneous reactions. Atmos. Chem. Phys. 15 (6), 2969–2983. https://doi.org/10.5194/acp-15-2969-2015.

Zheng, H., Song, S., Sarwar, G., Gen, M., Wang, S., Ding, D., Chang, X., Zhang, S., Xing, J., Sun, Y., Ji, D., Chan, C.K., Gao, J., McElroy, M.B., 2020. Contribution of particulate nitrate photolysis to heterogeneous sulfate formation for winter haze in China. Environ. Sci. Technol. Lett. 7 (9), 632–638. https://doi.org/10.1021/acs.estlett.0c00368.

Zhou, Y., Wang, T., Gao, X., Xue, L., Wang, X., Wang, Z., Gao, J., Zhang, Q., Wang, W., 2010. Continuous observations of water-soluble ions in PM2.5 at Mount Tai (1534 m

a.s.l.) in central-eastern China. J. Atmos. Chem. 64 (2–3), 107–127. https://doi.org/10.1007/s10874-010-9172-z.

Zhou, W., Xu, W., Kim, H., Zhang, Q., Fu, P., Worsnop, D.R., Sun, Y., 2020. A review of aerosol chemistry in Asia: insights from aerosol mass spectrometer measurements. Environ. Sci. Process Impacts 22 (8), 1616–1653. https://doi.org/10.1039/d0em00212g.

Zhu, W., Zhou, M., Cheng, Z., Yan, N., Huang, C., Qiao, L., Wang, H., Liu, Y., Lou, S., Guo, S., 2021. Seasonal variation of aerosol compositions in Shanghai, China: insights from particle aerosol mass spectrometer observations. Sci. Total Environ. 771, 144948 https://doi.org/10.1016/j.scitotenv.2021.144948.